Piezoelectric-Polarization-Enhanced Photovoltaic Performance in Depleted-Heterojunction Quantum-Dot Solar Cells

*Jian Shi, Ping Zhao, and Xudong Wang**

Colloidal quantum-dot (QD) photovoltaics (PVs) have shown a promising future with merits of low-cost processing, tunable spectral absorption, long-lifetime hot carriers, and multiple-exciton generation by a single photon.[1–5] For instance, tailoring the semiconductor bandgap of QDs by the quantum-size effect enables multijunction PVs in single-junction QD solar cells (QDSCs).[4] The ability of collecting hot carriers could theoretically raise the solar-energy-conversion efficiency of QDSCs to as high as 66%.[4,6] However, the performance of QDSCs is seriously hampered by the charge-extraction/transport problem due to the material and electrical discontinuity among organic molecule-capped QDs. Endeavors have been carried out to mitigate electron-hole recombination and improve the charge-extraction efficiency from various aspects. To alleviate charge recombination at the QD-anode interface, an ultradeep-work-function layer, such as MoO_3, was utilized to provide a back surface field to repel electrons.[7] Depletion-heterojunction (DH) QDSCs have been developed with a highest solar-energy-conversion efficiency of 7% using p-type QDs as absorbers and n-type wide-bandgap semiconductors as electron collectors.[8] The built-in electric field at the p-n junction effectively facilitates the dissociation of excitons and extraction of electrons from the QD thin film.[9] One critical obstacle for achieving highly efficient DH QDSCs is the divergence between their effective regions of charge extraction (effective depletion width ≈100–50 nm) and light absorption (≈1–2 μm thick film to fully absorb above-bandgap solar illumination).[10] Addressing this issue requires either a wider and steeper depletion region in the QD layer or a well-designed photomanagement structure of the charge-collecting electrode. Depletion bulk-heterojunction (DBH) QDSCs were exploited to reduce the compromise between light absorption and charge extraction using a porous charge collector.[11] However the very large QD/electrode interfacial area significantly increased the bimolecular recombination rate and thus reduced the charge-extraction efficiency.

A great number of studies have shown that the interfacial electronic band structure can be engineered by the permanent polarization induced by ionic displacement (e.g., the ferroelectric or piezoelectric effect).[12–17] This is typically implemented via strain either from lattice mismatching or mechanical deformation. In a heterojunction structure involving a piezoelectric semiconductor material, the appearance of a piezoelectric polarization (P_{pz}) will lead to a considerable change of the free-carrier distribution in both the piezoelectric material and its adjacent semiconductor or metal contacts. Accordingly, there will be a corresponding band structure change following the charge redistribution. The combination of P_{pz} and the redistribution of the free charge could effectively modulate the performance of practical heterojunction-based devices. For example, in wurtzite nitride-based quantum-well lasers, P_{pz} can largely deform the potential profile of the superlattice structure and affect the quantum efficiency by regulating the spatial overlapping between electrons and holes.[13] The application of P_{pz} to semiconductor functionalities has recently been explored to a much broader extent.[18–23] This interaction is denoted as the piezotronic effect, which implements a P_{pz}-induced charge redistribution to tune the interfacial band structure locally, and thus engineer the charge-transport properties without altering the interface structure or chemistry. Piezotronics has demonstrated great promise in augmenting the quantum efficiency of n-ZnO/p-GaN light-emitting diodes (LEDs), gating the nanowire-based field-effect transistor (FET), manipulating the metal-semiconductor contact type, and optimizing the interfacial band alignment in heterojunction systems.[20,24–26] Introducing the piezotronic concept to PV devices could also arbitrarily adjust the band structure at the interface, and thus modulate their performance. This unique capability may find great promise for improving the effectiveness of charge extraction in a QD-ZnO system. In this paper, we report the discovery of an enhanced performance of ZnO-PbS DH QDSCs by introducing P_{pz} at the heterojunction interface. Comprehensive experimental results evidence that screening P_{pz} can result in an expansion of the charge depletion region in a PbS QD film, and thus largely enhances exciton separation and charge extraction from the QDs. This strategy demonstrates a new route toward efficiency improvement of DH QDSCs.

Flexible DH QDSCs were constructed from an n-type ZnO thin film and p-type PbS QDs (Experimental Section). In a typical n-ZnO/p-PbS DH structure, the band offset ϕ_{bi} between the conduction bands of the ZnO and PbS serves as the driving force to separate photoexcited electron-hole pairs (**Figure 1**a). The built-in field in the depleted PbS layer ($\phi_{bi,PbS}$) provides the critical driving force for charge transfer through the barriers among the QDs (Figure 1b). Its magnitude and span are essential to charge extraction from the QD layer. An additional driving force could be expected when the interfacial charge redistribution is induced by P_{pz} from strained ZnO. Under a

J. Shi, Dr. P. Zhao, Prof. X. Wang
Department of Materials Science and Engineering
University of Wisconsin-Madison
Madison, WI 53706, USA
E-mail: xudong@engr.wisc.edu

DOI: 10.1002/adma.201203021

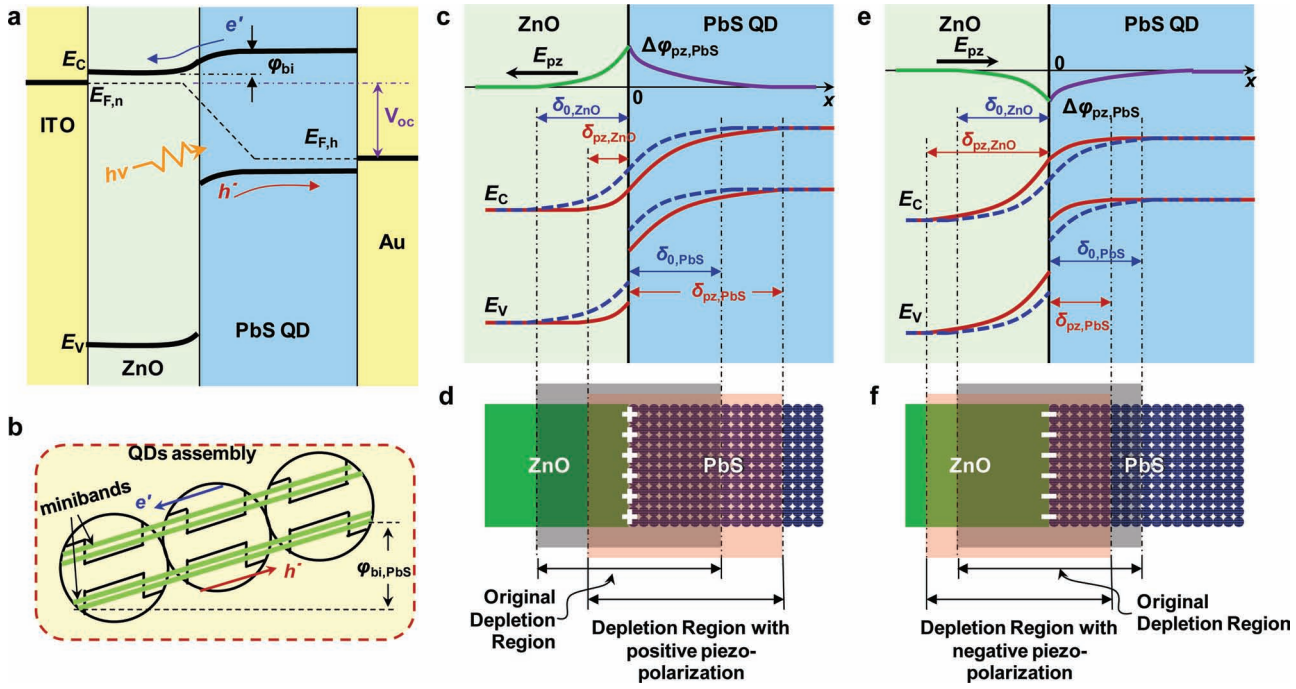

Figure 1. Working principle of QDSC subject to P_{pz}. a) Schematic drawing of band diagrams of a depletion-heterojunction QDSC, in which ZnO serves as the electron collector and Au as the hole collector. b) Material and electrical discontinuities occur at the interspaces of the QDs. The built-in potential $\phi_{bi,PbS}$ in the PbS QD layer is crucial for photoexcited charge separation and electron extraction. c) The tailoring of the QDSC band diagram when a positive P_{pz} appears at the ZnO/PbS interface: δ_0 and δ_{pz} denote the original and P_{pz}-modified width of the depletion regions, respectively. d) Schematic illustration of the change of the depletion regions in ZnO/PbS-QD assembly. e,f) The change of interface band structure (e) and depletion region (f), when negative P_{pz} appears at the ZnO/PbS interface. It is worthy of note that P_{pz}-induced interfacial band bending also exists at the ITO/ZnO side. However, the very short screening length of ITO (≈0.1 nm) makes the influence of charge redistribution at the ITO/ZnO interface negligible to charge transport.

steady strain, the ZnO thin film produces a permanent P_{pz}, which induces the redistribution of free charge carriers in ZnO, tin-doped indium oxide (ITO), and PbS to screen P_{pz}. According to Poisson's equation:[27]

$$\frac{d^2\varphi(x)}{dx^2} = -\frac{\rho(x)}{\varepsilon_0\varepsilon_r} \quad (1)$$

the change of the built-in potential profile, $\phi(x)$ can be derived based on the new charge distribution $\rho(x)$, as shown in the top graphs of Figure 1c,e. The maximum potential change in PbS is located at the interface ($\Delta\phi_{pz,PbS}$). In the ZnO/PbS QDSCs, $\Delta\phi_{pz,PbS}$ exhibited a linear relationship with the applied strain (≈0.13V per 0.1% strain, Supporting Information, Figure S2). The comparable magnitude of $\Delta\phi_{pz,PbS}$ to the original p-n junction built-in potential (≈0.6 V) suggests a good possibility of effective band-structure engineering.Therefore, as shown in the bottom graphs of Figure 1c,e, the original space-charge-induced band structure of the ZnO/PbS p-n junction (blue dashed lines) is modulated by the extra potential generated by the P_{pz}-induced charge redistribution in the PbS and ZnO (red solid lines). When a positive P_{pz} appears at the ZnO/PbS interface, both the conduction and the valence bands of the PbS are bent further downward producing a sharper and extended built-in field, which is preferable for sweeping excitons apart. In this scenario, the driving force for electron extraction from the PbS-QD assembly is augmented to be $\phi_{bi,PbS} + \Delta\phi_{pz,PbS}$ and the width of the depletion region in PbS under zero external bias is expanded to:[14,27]

$$\delta_{pz,PbS} = \sqrt{\frac{2\varepsilon_0\varepsilon_r(\varphi_{bi,PbS} + \Delta\varphi_{pz,PbS})}{q\,N_{PbS,eff}}} \quad (2)$$

where $N_{PbS,eff}$ is the effective carrier concentration including contributions from interface defects and surface states. This enlarged depletion region in the PbS QD layer is imperative for enhanced charge extraction. Meanwhile, the positive P_{pz} may also yield a shorter depletion region ($\delta_{pz,ZnO}$) and shallower band bending on the ZnO side. The overall change of the depletion region at the ZnO/PbS interface is schematically illustrated in Figure 1d. Because the electron mobility in p-type discrete PbS QDs is far worse than that in n-type ZnO, the enhancement of the electron extraction in the PbS region should be the overwhelming effect in regulating the overall performance of ZnO/PbS junctions. Therefore, positive P_{pz} at the ZnO/PbS interface is a favorable condition for charge extraction. Similarly, when a negative P_{pz} appears at the interface, as shown in Figure 1e,f, the band offset reduces to ($\phi_{bi,PbS} - \Delta\phi_{pz,PbS}$) and the depletion region in the PbS shrinks ($\delta_{pz,PbS} < \delta_{0,PbS}$). Therefore, the charge-extraction capability is jeopardized and a lower PV efficiency is expected.

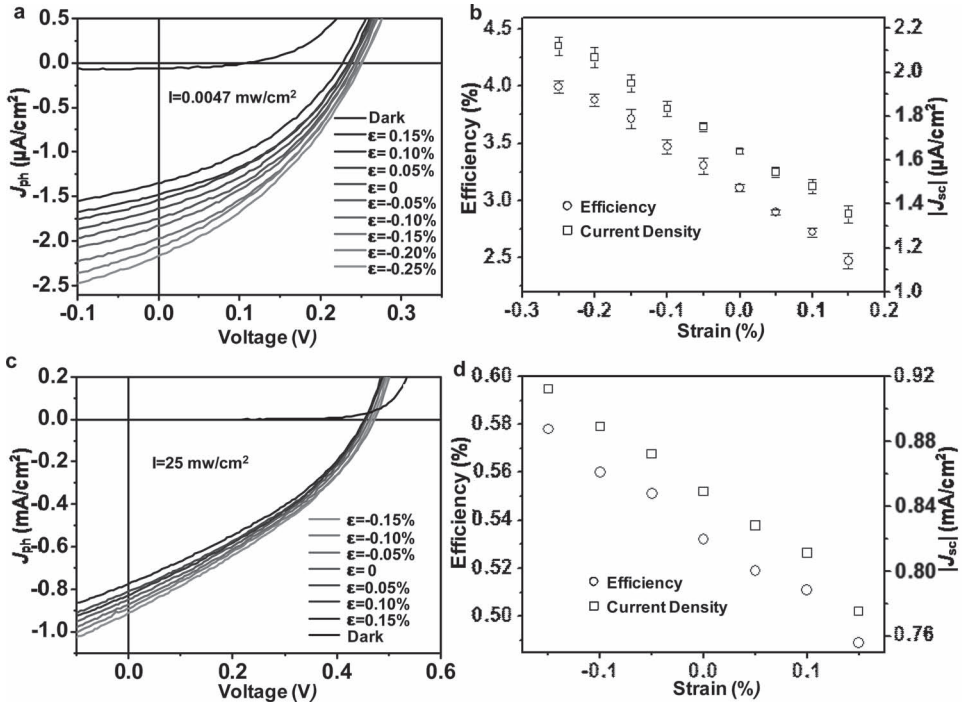

Figure 2. Strain-related performances of a QDSC. a) *J–V* characteristics of a ZnO/PbS QDSC collected under 0.0047 mW cm^{-2} illumination, when the cell was subjected to different compressive and tensile strains. b) Plot of QDSC efficiency (open circles) and J_{sc} (open squares) as a function of strain. An approximately linear relationship can be observed. c,d) *J–V* characteristics (c) and J_{sc}–strain relationships (d), when the QDSC was measured under 25 mW cm^{-2} light intensity. Similar trends were observed for efficiency–strain and J_{sc}–strain relationships though with lower slopes.

The performance of the ZnO/PbS QDSCs was characterized as a function of strain to investigate the influence of P_{pz}. The dark-current density of the cell was found to be ≈–100 nA cm^{-2} under reverse bias, indicating a good diode property. It has been shown that, under illumination, photoexcited carriers can be trapped at the interfacial defects/states, which reduces the width of the depletion region and impedes charge extraction.[28] Therefore, in order to manifest the influence of P_{pz} to the greatest extent possible and avoid unnecessary screening effects from defects or surface states, the QDSCs were first characterized under very low light intensity. Under the illumination of a 0.0047 mW cm^{-2} simulated solar spectrum, an appreciable J_{ph} change was discovered. **Figure 2**a shows the J_{ph}–*V* curves of the QDSC under different strains. A linear relationship was identified from the plot of J_{sc} versus strain (open squares in Figure 2b), where J_{sc} exhibited a 0.02 μA cm^{-2} (or 1.1%) increase per 0.01% strain drop. Because compressive and tensile strains generated positive and negative P_{pz} at the ZnO/PbS interface, respectively (Supporting Information, Figure S2), the observed J_{sc} changes were consistent with the modulation model presented in Figure 1.

The solar-energy-conversion efficiencies were calculated from the *J–V* curves and plotted as a function of strain (open circles in Figure 2b). Under zero strain, the efficiency of the QDSC was ≈3.1%. An efficiency of ≈4.0% was obtained at a compressive strain of –0.25%, corresponding to an improvement of ≈30%. The efficiency also exhibited an approximately linear relationship with strain within the testing range (–0.25%–0.15%), where a 1.2% efficiency enhancement per 0.01% strain drop was identified.

The QDSC was further tested under a higher illumination flux to investigate the effectiveness of P_{pz} modulation when the screening effect became significant. Figure 2c shows the strain-related *J–V* curves of the QDSC under 25 mW cm^{-2} illumination. J_{sc} and the efficiency of the QDSC exhibit the same changing trends as those obtained under weak illumination, whereas the percentages of J_{sc} and the efficiency change per 0.01% strain were only 0.51% and 0.55%, respectively (Figure 2d). This observation demonstrates that a pronounced screening effect from trapped photoexctied charges could diminish the P_{pz}-modulated interfacial depletion-region variation, and thus reduce the degree of PV performance change. It is important to note that the photoexcited charges themselves do not screen P_{pz}. What screens P_{pz} are the charged surface or bulk trap states formed under a high flux of the photocurrent due to the slow charge-transfer kinetics on these defective states.[28] This phenomenon is similar to the light-intensity-dependent PV performance observed in many SC systems, where higher efficiency is typically obtained at low illumination intensity.[29–31] This is because the high density of charged surface and trap states resulting from a high illumination intensity often reduces the effective depletion region in a PbS absorber, facilitates electron-hole recommendation, and therefore jeopardizes the quantum efficiency of QDSCs. At low illumination intensity (such as 0.0047 mW cm^{-2}, that used in our experiments), the surface and trap states are rarely charged due to the low flux

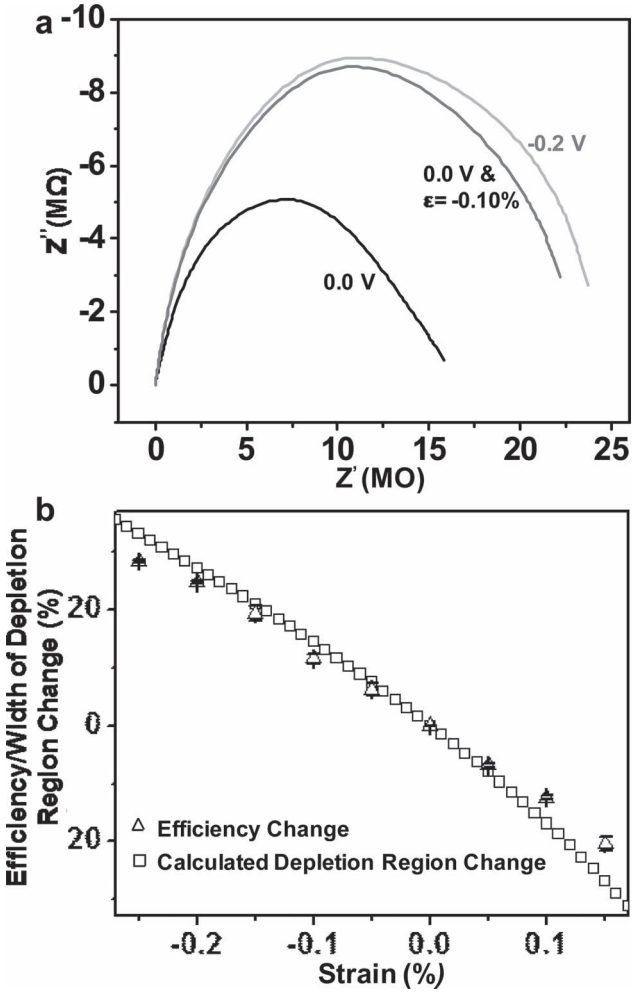

Figure 3. Depletion-region characterization. a) Electrochemical impedance spectroscopy measurements of the QDSC under reverse bias and strain. Applying a reverse bias of –0.2 V was found to give a similar impedance spectrum as that obtained under zero bias but with a –0.10% strain. b) Computed change of width of depletion region as a function of strain (built-in potentials are collected from Figure S2 in the Supporting Information) and measured efficiency change versus strain. A strong correlation can be identified between these two sets of data.

of photocurrent, and thus their impedance to charge extraction and transport is minimized. This light-intensity dependence of the PV performance could be largely or even completely suppressed by improving the quality of the QDs and the QD-ZnO interfaces.[32] Similarly, this strategy also applies to minimizing the light-intensity influence on the observed P_{pz} modulation, and thus maximizing the P_{pz}-induced efficiency gain of PV systems under high light intensity.

To obtain a more quantitative understanding of the depletion region under the influence of P_{pz}, electrochemical impedance spectroscopy (EIS) was applied to analyze the internal electrical parameters of the QDSC (Supporting Information, Figure S3). In the low-frequency range, the QDSC can be fitted to a simple *RC* circuit (*R* and *C* are in parallel) to model the impedance of the PbS/ZnO interface, where *R* is the series resistance, and *C* is the specific capacitance of the depletion region.[33] The observed low impedance demonstrates a well-defined interface of the QDSC. Therefore, Nyquist plots under reverse bias can be applied to quantify the *C* and the width of depletion region ($C = \varepsilon_{junction}/\delta_{junction}$, Supporting Information, S3).

Figure 3a shows the impedance spectra of the ZnO/PbS interface. When only a –0.10% strain (corresponding to ≈–0.25 V $\Delta\phi_{pz,PbS}$, as obtained from Figure S2 in the Supporting Information) was applied to the QDSC, the impedance spectrum exhibited a shape very close to that obtained under –0.2 V reverse bias. This result proves that strain-induced polarization and externally applied bias can equivalently modulate the depletion region at the PbS/ZnO interface. With this evidence, the change of the depletion region in PbS was calculated based on the piezoelectric potential measured under different strains (Supporting Information, S3). Figure 3b plots the percentage of the calculated depletion-region change together with the measured efficiency change (collected from Figure 2b) as functions of strain. It clearly shows that cell efficiency has a strong correlation with the width of the depletion region, suggesting that performance change of the QDSC was mainly a result of the P_{pz}-induced depletion-region variation in PbS.

To verify further this conclusion, a control experiment was conducted, where the thickness of ZnO layer was increased from 200 nm to 920 nm. The thicker ZnO layer generated a higher P_{pz} at the interface (Supporting Information, Figure S4) but retarded electron diffusion. As expected, the 920 nm ZnO film yielded a much lower PV efficiency (under 0.0047 mW cm^{-2} illumination) compared with the 200 nm ZnO-based QDSCs (Supporting Information, Figure S5). However, the efficiency change per unit strain drop was significantly larger since a much higher P_{pz} could be produced by the 920 nm ZnO film under the same strain. A PV efficiency increase of 144% was observed at a compressive strain of –0.25%, which was more than three times higher than that obtained from the 200 nm ZnO devices.

In order to fully reveal the P_{pz}-modulated QDSC performance change, open-circuit voltage (V_{oc}) was further investigated. Under weak illumination (0.0047 mW cm^{-2}), where significant J_{sc} change was observed, the change of V_{oc} (ΔV_{oc}) exhibited an approximately linear relationship with strain (≈0.9 mV per 0.01% strain, black squares in **Figure 4**a). The strain-related V_{oc} changes were constant, rather than the piezopotential spikes as those obtained from typical piezoelectric devices (Supporting Information, Figure S6). The change of V_{oc} could first be attributed to J_{sc} variation via Equation 3:[27,34]

$$V_{OC} = \frac{nkT}{e} \ln\left(\frac{J_{SC}}{J_0}\right) \quad (3)$$

where *n* is the ideality factor and J_o is dark-current density. The prefactor nkT/e was found to be ≈40 mV (with $n = 1.55$) from the *J–V* characteristics under different light intensities (Supporting Information, Figure S7), in which the V_{oc} change was merely a result of J_{sc}. Based on Equation 3, ΔV_{oc} was calculated using J_{sc} obtained from the *J–V* characteristics shown in Figure 2a. The calculated ΔV_{oc} also exhibited a linear relationship with strain, but with a smaller slope (≈0.5 mV per 0.01% strain, open circles in Figure 4a) compared with the measured ones. This

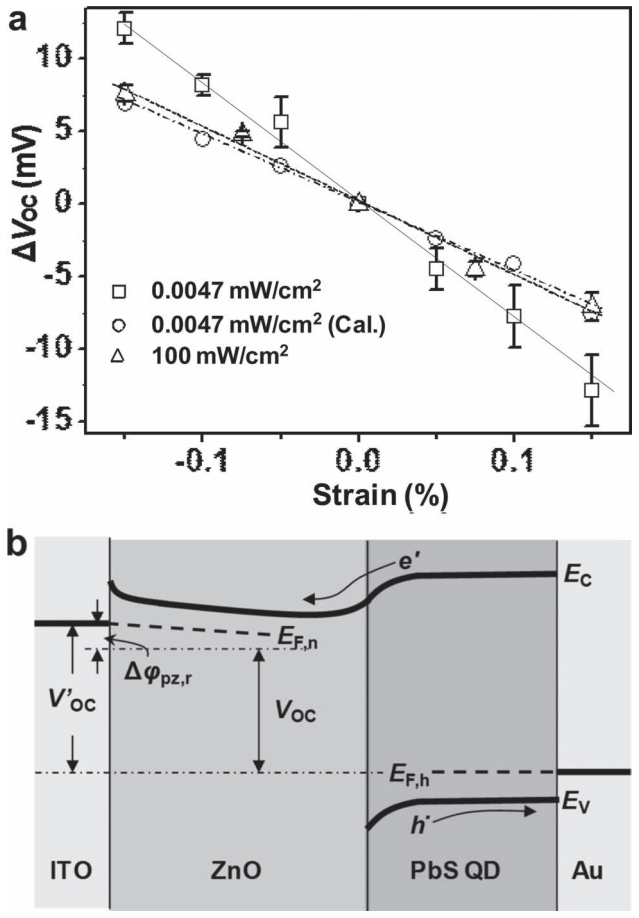

Figure 4. Investigation of V_{oc} change in response to P_{pz}. a) ΔV_{oc} and strain relationships measured under weak illumination (0.0047 mW cm^{-2}) (squares), strong illumination (100 mW cm^{-2}) (triangles), and calculated based on ΔJ_{sc} measured under weak illumination (circles). Linear relationships could be identified from all these three sets of data, where the slopes are 0.9 mV ΔV_{oc} per 0.01% strain change, 0.5 mV ΔV_{oc} per 0.01% strain change, and 0.5 mV ΔV_{oc} per 0.01% strain change, respectively. b) A schematic drawing of ITO-ZnO-PbS band diagram illustrating the contribution from the remnant piezopotential to ΔV_{oc}.

discrepancy suggests that an additional effect, such as the remnant piezopotential at the ITO/ZnO interface, may contribute to ΔV_{oc} as well.

The role of the remnant piezopotential in ΔV_{oc} was illustrated by characterizing the QDSC under strong illumination (100 mW cm^{-2}), which could significantly increase the density of charged surface states (or the effective charge-carrier concentration, $N_{PbS,eff}$) at the ZnO/PbS interface, and curtail the P_{pz}-induced expansion of the depletion region (Supporting Information, Figure S8). The density of charged surface states was quantitatively higher than the P_{pz} that appeared on the strained ZnO surface, and a complete screening of P_{pz} resulted. Therefore, J_{sc} of the QDSC measured under 100 mW cm^{-2} was nearly non-responsive to P_{pz}, whilst small changes of V_{oc} during straining were still obtained (≈0.5 mV per 0.01% strain, triangles in Figure 4a). Under this situation, the V_{oc} change was not related to J_{sc} and was solely contributed by the remnant piezopotential at the ITO/ZnO interface, $\Delta\phi_{pz,r}$. This was the same case as the piezopotential-induced V_{oc} variation observed from ZnO-polymer SCs.[34] This effect can be understood by the band alignment of ITO, ZnO, and PbS under compressive strain (Figure 4b). In the open-circuit state, the piezopotentials on both sides of ZnO will be partially screened by the redistributions of holes in PbS and free electrons in ITO electrodes. The finite carrier concentration and density of states, however, could result in a considerable unscreened remnant potential ($\Delta\phi_{pz,r}$) at the ITO/ZnO interface, which shifts the electron quasi Fermi level in the ITO electrode accordingly. This remnant piezopotential is only related to the physical properties of the materials that form the heterojunctions and always exists regardless of the incident light intensity. Adding this effect (≈0.5 mV per 0.01% strain) to the calculated ΔV_{oc}–ε relationship under low light intensity (≈0.5 mV per 0.01% strain) can approximately recover the experimentally determined result (≈0.9 mV per 0.01% strain), evidencing the combined two contributions to ΔV_{oc}.

In summary, we report a novel strategy to modulate the interfacial band structure of ZnO/PbS QDSCs by P_{pz}. The enhancement of J_{sc} and efficiency was mostly due to the expansion of the depletion region in PbS, as a result of P_{pz}-induced charge redistribution at the ZnO/PbS interface. The change of V_{oc} was less significant and consisted of two components: photocurrent-related quasi Fermi level shifting and the remnant piezopotential at the ZnO/ITO interface. The PV performance became less responsive to P_{pz} under a higher illumination intensity due to the compensation from trapped photoexcited charges at the interface. The illumination-intensity-dependent P_{pz} enhancement shares the same mechanism as illumination-intensity-dependent PV performance. Therefore, prominent enhancement could be expected under strong illumination when the interface defects are minimized and fast charge-transfer kinetics are achieved. This situation is highly desirable for PV-device development, and can be realized by carefully designing and fabricating high-quality interfaces. The piezotronic modulation strategy endows new insights for improving the PV efficiency of QDSCs and sheds light on engineering the electrical-transport properties of heterojunction devices by introducing P_{pz}.

Experimental Section

Materials: (0001)-oriented texture ZnO film was deposited in a radio-frequency (RF) sputtering system. Prior to deposition, the as-received ITO/poly(ethylene terephthalate) (PET) substrate (from Multek; the ITO layer was 200 nm thick and the PET was 75 μm thick) was cleaned by acetone, ethanol, and deionized (DI) water in sequence and dried by N_2. A 2 inch × 2 inch substrate was used for ZnO sputtering at a pressure of 1.5×10^{-3} Torr under Ar (50 sccm) and O_2 (15 sccm) flow. The RF power for sputtering was kept at 80 W. Deposition was paused every 30 min for a 30 min period to prevent overheating the substrate. The total deposition time was 250 min for a thickness of ≈1 μm. The as-received PbS QDs were p-type and their surfaces were capped with oleic acid. Before processing, all of the QDs were subjected to five rounds of intensive precipitation and centrifugation with acetone and 1-butanol or methanol. Then, the QDs were dispersed in hexane at 25 mg mL^{-1} for the dip-coating.

Device Fabrication: As-received, either two different sizes of a p-type PbS QDs (Test Kit from Evident Technologies) mixture (with absorption

edges at 850 nm and 1100 nm) or single-sized QDs with absorption at 1500 nm were deposited on a 20 mm × 10 mm ZnO substrate by the layer-by-layer dip-coating method, typically 25 times. Each cycle includes three steps: 20 s dip-coating in QD solution, 60 s dip-coating in 5% 1,2-ethanedithiol (EDT)/acetonitrile solution and 3 s dip-coating in acetonitrile. Between each step, the samples were allowed to dry completely under the ambient atmosphere. Then, the Au electrode pads (from 0.5 mm^2 to 0.78 mm^2) were deposited by electron-beam evaporation with a thickness of 100 nm, in which a shadow mask was applied. The complete QDSCs were anchored on a home-made PMMA clamp, where the working area of the cell was right above the clamped point. Thus, the strain experienced by the ZnO could be quantified via the traditional cantilever model.

Photovoltaic Measurements: A potentiostat (Solartron SI 1287) was applied to monitor the current density versus applied bias under different strains. The light source was a 500 W Hg (Xe) arc lamp (Oriel, 66142) with an AM1.5G filter. An IR filter (Oriel, 6123NS) was applied to eliminate the IR heating effect. Prior to electrical characterization, the QDSCs were illuminated by UV light for 30 min to escalate the carrier concentration of ZnO by the photodoping method. During the measurement, the ITO side of the sample faced the light source. A speed-controlled motor with a wedged shaft was used to introduce strains toward the QDSCs in a well-controlled manner.

Electrical Impedance Spectroscopy (EIS) Measurements: The EIS measurements were conducted using an SI 1260 Impedance/Gain-Phase Analyzer. The AC amplitude applied was 50 mV. Nyquist plots of the QDSC were obtained in the frequency range from 0.1 Hz to 1 MHz.

Supporting Information

Supporting Information is available from the Wiley Online Library or from the author.

Acknowledgements

The authors thank financial support from DARPA under grant No. N66001-11-1-4139, the National Science Foundation under grant No. DMR-0905914, and the UW-Madison graduate school.

Received: July 25, 2012
Revised: September 14, 2012
Published online: November 26, 2012

[1] R. Debnath, O. Bakr, E. H. Sargent, *Energy Environ. Sci.* **2011**, *4*, 4870.
[2] P. V. Kamat, *J. Phys. Chem. C* **2008**, *112*, 18737.
[3] I. J. Kramer, E. H. Sargent, *ACS Nano* **2011**, *5*, 8506.
[4] E. H. Sargent, *Nat. Photonics* **2012**, *6*, 133.
[5] A. J. Nozik, *Inorg. Chem.* **2005**, *44*, 6893.
[6] W. A. Tisdale, K. J. Williams, B. A. Timp, D. J. Norris, E. S. Aydil, X. Y. Zhu, *Science* **2010**, *328*, 1543.
[7] P. R. Brown, R. R. Lunt, N. Zhao, T. P. Osedach, D. D. Wanger, L. Y. Chang, M. G. Bawendi, V. Bulovic, *Nano Lett.* **2011**, *11*, 2955.
[8] A. H. Ip, S. M. Thon, S. Hoogland, O. Voznyy, D. Zhitomirsky, R. Debnath, L. Levina, L. R. Rollny, G. H. Carey, A. Fischer, K. W. Kemp, I. J. Kramer, Z. Ning, A. J. Labelle, K. W. Chou, A. Amassian, E. H. Sargent, *Nat. Nanotechnol.* **2012**, *7*, 577.
[9] S. M. Willis, C. Cheng, H. E. Assender, A. A. R. Watt, *Nano Lett.* **2012**, *12*, 1522.
[10] D. A. R. Barkhouse, I. J. Kramer, X. H. Wang, E. H. Sargent, *Opt. Express* **2010**, *18*, A451.
[11] D. A. R. Barkhouse, R. Debnath, I. J. Kramer, D. Zhitomirsky, A. G. Pattantyus-Abraham, L. Levina, L. Etgar, M. Gratzel, E. H. Sargent, *Adv. Mater.* **2011**, *23*, 3134.
[12] T. F. Kuech, R. T. Collins, D. L. Smith, C. Mailhiot, *J. Appl. Phys.* **1990**, *67*, 2650.
[13] S. H. Park, S. L. Chuang, *J. Appl. Phys.* **1998**, *72*, 3103.
[14] L. Pintilie, M. Alexe, *J. Appl. Phys.* **2005**, *98*, 124103.
[15] V. M. Voora, T. Hofmann, M. Brandt, M. Lorenz, M. Grundmann, N. Ashkenov, H. Schmidt, N. Ianno, M. Schubert, *Phys. Rev. B* **2010**, *81*, 195307.
[16] Y. Watanabe, *Phys. Rev. B* **1998**, *57*, 789.
[17] P. Zubko, D. J. Jung, J. F. Scott, *J. Appl. Phys.* **2006**, *100*, 114112.
[18] X. D. Wang, J. Zhou, J. H. Song, J. Liu, N. S. Xu, Z. L. Wang, *Nano Lett.* **2006**, *6*, 2768.
[19] Z. L. Wang, *Nano Today* **2010**, *5*, 540.
[20] W. Z. Wu, Y. G. Wei, Z. L. Wang, *Adv. Mater.* **2010**, *22*, 4711.
[21] Y. Zhang, Y. Liu, Z. L. Wang, *Adv. Mater.* **2011**, *23*, 3004.
[22] Y. Zhang, Y. Yang, Z. L. Wang, *Energy Environ. Sci.* **2012**, *5*, 6850.
[23] J. Shi, M. B. Starr, X. D. Wang, *Adv. Mater.* **2012**, *24*, 4683.
[24] J. Shi, M. B. Starr, H. Xiang, Y. Hara, M. A. Anderson, J. H. Seo, Z. Q. Ma, X. D. Wang, *Nano Lett.* **2011**, *11*, 5587.
[25] Q. Yang, W. H. Wang, S. Xu, Z. L. Wang, *Nano Lett.* **2011**, *11*, 4012.
[26] J. Zhou, P. Fei, Y. D. Gu, W. J. Mai, Y. F. Gao, R. Yang, G. Bao, Z. L. Wang, *Nano Lett.* **2008**, *8*, 3973.
[27] S. M. Sze, K. K. Ng, *Physics of Semiconductor Devices*, Wiley, Hoboken, NJ, USA **2007**.
[28] J. Bisquert, G. Garcia-Belmonte, A. Munar, M. Sessolo, A. Soriano, H. J. Bolink, *Chem. Phys. Lett.* **2008**, *465*, 57.
[29] I. N. Mora-Seró, S. Giménez, F. Fabregat-Santiago, R. Gómez, Q. Shen, T. Toyoda, J. Bisquert, *Acc. Chem. Res.* **2009**, *42*, 1848.
[30] M. Qin, K. Yao, Y. C. Liang, B. K. Gan, *Appl. Phys. Lett.* **2007**, *91*, 092904.
[31] T. Berger, T. Lana-Villarreal, D. Monllor-Satoca, R. Gómez, *J. Phys. Chem. C* **2007**, *111*, 9936.
[32] M. Grätzel, R. A. J. Janssen, D. B. Mitzi, E. H. Sargent, *Nature* **2012**, *488*, 304.
[33] L. Etgar, T. Moehl, S. Gabriel, S. G. Hickey, A. Eychmuller, M. Grätzel, *ACS Nano* **2012**, *6*, 3092.
[34] Y. Yang, W. X. Guo, Y. Zhang, Y. Ding, X. Wang, Z. L. Wang, *Nano Lett.* **2011**, *11*, 4812.